Proteomic signatures of extracellular vesicles secreted by nonmineralizing and mineralizing human osteoblasts and stimulation of tumor cell growth

Jess Morhayim,* Jeroen van de Peppel,* Jeroen A. A. Demmers,† Gulistan Kocer,* Alex L. Nigg,‡ Marjolein van Driel,* Hideki Chiba,§ and Johannes P. van Leeuwen*,[1]

*Department of Internal Medicine and Erasmus MC Stem Cell and Regenerative Medicine Institute, †Proteomics Center, and ‡Department of Pathology, Erasmus University Medical Center, Rotterdam, The Netherlands; and §Department of Basic Pathology, Fukushima Medical University School of Medicine, Hikarigaoka, Fukushima, Japan

ABSTRACT **Beyond forming bone, osteoblasts play pivotal roles in various biologic processes, including hematopoiesis and bone metastasis. Extracellular vesicles (EVs) have been implicated in intercellular communication *via* transfer of proteins and nucleic acids between cells. We focused on the proteomic characterization of nonmineralizing (NMOBs) and mineralizing (MOBs) human osteoblast (SV-HFOs) EVs and investigated their effect on human prostate cancer (PC3) cells by microscopic, proteomic, and gene expression analyses. Proteomic analysis showed that 97% of the proteins were shared among NMOB and MOB EVs, and 30% were novel osteoblast-specific EV proteins. Label-free quantification demonstrated mineralization stage-dependent 5-fold enrichment of 59 and 451 EV proteins in NMOBs and MOBs, respectively. Interestingly, bioinformatic analyses of the osteoblast EV proteomes and EV-regulated prostate cancer gene expression profiles showed that they converged on pathways involved in cell survival and growth. This was verified by *in vitro* proliferation assays where osteoblast EV uptake led to 2-fold increase in PC3 cell growth compared to cell-free culture medium–derived vesicle controls. Our findings elucidate the mineralization stage-specific protein content of osteoblast-secreted EVs, show a novel way by which osteoblasts communicate with prostate cancer, and open up innovative avenues for therapeutic intervention.—Morhayim, J., van de Peppel, J., Demmers, J. A. A., Kocer, G., Nigg, A. L., van Driel, M., Chiba, H., van Leeuwen, J. P. Proteomic signatures of extracellular vesicles secreted by nonmineralizing and mineralizing human osteoblasts and stimulation of tumor cell growth. *FASEB J.* 29, 274–285 (2015). www.fasebj.org**

Key Words: bioactivity · intercellular communication · prostate cancer · protein cargo

OSTEOBLASTS ARE THE BONE CELLS of mesenchymal origin that contribute to the strength of the skeletal system by bone matrix production and mineralization (1, 2). The discovery of various cytokines and chemokines secreted by osteoblasts have underlined the importance of paracrine signaling in the establishment of favorable microenvironments that support the regulation of bone homeostasis as well as the growth, survival, and maintenance of neighboring bone marrow cells (3, 4). In cancer, the osteoblastic microenvironment acts as a premetastatic niche by attracting bone-metastasizing tumors (5, 6). Identifying the regulatory mechanism of osteoblast paracrine signaling network may help us design therapeutics to reduce the risk of bone disorders and metastases.

Extracellular vesicles (EVs) have emerged as a novel class of cellular messengers involved in communication *via* exchange of bioactive cargo, such as lipids, proteins, and nucleic acids, among cells (7, 8). EVs are released under physiologic and pathologic conditions, and they are involved in various developmental and biologic processes as well as in disease progression (9, 10). Thanks to their bioactive content and biocompatibility, EVs have been of increasing interest for their applications as biomarkers, vaccines, and drug-delivery agents (11–13). Although there are no defined terms yet to classify different types of EVs, 3 processes of EV biogenesis have been well documented. Exocytosis of multivesicular bodies releases small vesicles (10–100 nm) called exosomes and exosome-like vesicles (14). Budding from the plasma membrane releases a heterogeneous group of vesicles (100–1000 nm), usually referred to as microvesicles (15). Cells undergoing apoptosis also release EVs as apoptotic bodies (0.8–5 μm) formed by the breakdown of dying cells (16). Osteoblasts secrete EVs called matrix vesicles (30–300 nm), which are mainly involved in mineralization of the newly forming bone matrix *via* hydroxyapatite deposition (17). Reports describing the protein profiles of matrix vesicles secreted by osteoblast cell lines from different species indicated that they contain a broad variety of proteins important for bone mineralization (18–20). However,

Abbreviations: EV, extracellular vesicles; MOB, mineralizing osteoblasts; NMOB, nonmineralizing osteoblasts

[1] Correspondence: Department of Internal Medicine, Erasmus University Medical Center, Wytemaweg 80, 3015 CN, Rotterdam, The Netherlands. E-mail: j.vanleeuwen@erasmusmusmc.nl

doi: 10.1096/fj.14-261404

This article includes supplemental data. Please visit *http://www.fasebj.org* to obtain this information.

0892-6638/15/0029-0274 © FASEB

there a few studies demonstrate that matrix vesicles contain signaling proteins and growth factors, such as BMPs and VEGF, suggestive of a role in intercellular communication (21). However, comprehensive information about osteoblast-secreted EVs with roles other than mineralization is still lacking.

In this study, we extensively characterized human osteoblast-secreted EVs in terms of size, morphology, and protein content. We report their role in communication with bone-metastasizing human prostate cancer cells. We focused on identifying the unique and abundant proteins packaged within EVs secreted at various time points during osteoblast differentiation under both mineralizing and nonmineralizing conditions. We also delineated the biologic function of osteoblast EVs by showing that they enter human prostate cancer (PC3) cells and stimulate their growth *in vitro*. Our findings define a role for osteoblast EVs in intercellular communication and provide a foundation for the development and utilization of EVs as treatment agents.

MATERIALS AND METHODS

Cell culture

Simian virus 40 immortalized human osteoblast cell line (SV-HFO cells) established from normal human fetal calvaria was cultured as described previously with modifications (22). Cell culture medium was supplemented with FCS (Gibco, Paisley, United Kingdom) that was depleted of serum-derived EVs by ultracentrifugation at 100,000*g* 90 min, 4°C). PC3 cells were cultured in α-MEM (Gibco) supplemented with streptomycin/penicillin, 1.8 mM $CaCl_2$ (Sigma-Aldrich, St. Louis, MO, USA), and 10% FCS at 37°C. For functional experiments, PC3 cell culture medium was supplemented with 2% FCS.

Extracellular vesicle isolation

SV-HFOs were refreshed with serum-free medium before EV isolation. After 24 h, the conditioned medium was subjected to low-speed centrifugation (1500 rpm, 5 min; 4500 rpm, 10 min) followed by ultracentrifugation (20,000*g*, 30 min; 100,000*g*, 1 h at 4°C) using a SW28 rotor (Beckman Coulter, Fullerton, CA, USA). The 100,000*g* EV pellet derived from 20 ml conditioned medium was resuspended in 20 μl fixative for TEM, 100 μl PBS for biochemical assays and immunoblotting, and 100 μl PC3 culture medium for functional experiments. EVs were labeled with PKH67 (Sigma-Aldrich) according to the manufacturer's instructions. The amount of experimental EV dose was determined (%, v/v). Cell- and serum-free SV-HFO culture medium was processes the same way as the conditioned medium and was used as a control for functional experiments.

Biochemical assays

Alizarin staining, protein concentration, alkaline phosphatase (ALPL) activity assay, and DNA quantification were performed as described previously (23). In brief, mineralization of the bone matrix was monitored by Alizarin Red staining of the calcium matrix. Cells were fixed with 70% ethanol for 60 min on ice. After fixation, cells were washed with 1× PBS twice and stained with Alizarin Red solution (saturated Alizarin Red in demineralized water titrated to pH 4.2 with 0.5% ammonium hydroxide) for 10 min. Protein concentration was determined using the BCA kit (Pierce Biotechnology, Rockford, IL, USA) following the manufacturer's instructions. ALPL activity of the whole-cell lysates and EVs was determined in a colorimetric assay detecting the release of paranitrophenol from paranitrophenyl phosphate upon reaction catalyzed by endogenous ALPL. The activity was displayed as enzyme units per milligrams of total protein. DNA was quantified by spectrofluorometry using ethidium bromide. Samples were analyzed by a microplate reader using an excitation filter of 340 nm and an emission filter of 590 nm.

Immunoblot analysis

Protein samples were prepared by mixing the EVs (in PBS) with 6× reducing sample buffer immediately after isolation. EV proteins (3 μg total protein per sample) were separated by SDS-PAGE at 200 V and transferred onto a nitrocellulose membrane (Hybond-ECL; Amersham Biosciences, Buckinghamshire, United Kingdom). After blocking nonspecific signal with 5% BSA in TBS/0.1% Tween-20, the membrane was incubated with primary antibodies against annexin A2 (rabbit polyclonal antibody, 1:500; Abcam, Cambridge, United Kingdom) and CD63 (rabbit polyclonal antibody, 1:1000; Santa Cruz Biotechnology, Dallas, TX, USA). Membranes were probed with secondary antibody conjugated with IRDye 800CW (1:5000, goat anti-rabbit; Li-Cor, Lincoln, NE, USA) using Odyssey Infrared Imaging System according to the manufacturer's instructions (Li-Cor).

Flow cytometry

PC3 cells were incubated with different concentrations (% v/v) of PKH67-labeled day 12 osteoblast EVs and EV control. After overnight culture, the mean fluorescence intensity was detected by flow cytometry (BD Accuri C6; BD Biosciences, San Jose, CA, USA) using the FITC channel. Absolute cell counts were determined using counting beads (BD Biosciences).

Transmission electron microscopy

EVs were fixed in 4% formaldehyde (37% solution; Merck, New York, NY, USA) in 1% glutaraldehyde (25% solution, Merck) at 4°C (Trump fixative). Fixative was removed by incubating the sample in Millonig buffer ($NaH_2PO_4 \cdot H_2O$) (BDH Chemicals, Radnor, PA, USA) for 6 h, followed by postfixation with 1% osmium tetroxide (4% solution; Electron Microscopy Sciences, Hatfield, PA, USA). The samples were rinsed with distilled water and a series of acetone concentrations (50%, 70%, 90%, 96%, 100%). The EV pellets were incubated on pure epoxy resin for 1 h at 37°C, then embedded in fresh epoxy and polymerized for 12 h at 60°C. The polymerized resin was cut into thin sections (40–60 nm) with an ultramicrotome (Ultracut UCT; Leica, Wetzlar, Germany) and a diamond knife (Diatome, Hatfield, PA, USA) and mounted on a copper grid. The sample was detected by transmission electron microscopy (Morgagni; Philips/FEI, Hillsboro, OR, USA).

4Pi microscopy

EV uptake by PC3 cells was monitored using a 4Pi microscope, which is a confocal fluorescence microscope with an improved axial resolution by a factor of 5 to 7 over conventional confocal microscopes (24). PC3 cells were seeded on poly-L-lysine-coated quartz coverslips. After overnight incubation with PKH67-labeled

EVs, cells were washed with PBS, fixed with 10% formalin, and stained with concanavalin A (Alexa Fluor 647 conjugate; Life Technologies, Carlsbad, CA, USA). The fixed cells were washed 3 times with 0.01 M PBS and then impregnated 3 times with glycerol 87%. The coverslip was mounted on a special 4Pi sample holder and covered with another quartz coverslip, using glycerol 87% as mounting medium, giving the whole beam path a refractive index of 1.458 (25). The coverslips were sealed with 2-component silicon (Picodent Twinsil; Wipperfürth, Germany). Images were taken with a Leica 4Pi TCS microscope using two opposing ×100 1.35 NA glycerol HCX PL APO objectives. A 2-photon Ti-sapphire laser (Mai Tai; Spectra Physics, Santa Clara, CA, USA) was used for excitation at a wavelength of 800 nm (26). Avalanche photo diodes were used for detection of the signals with a 500 to 550 nm bandpass filter for PKH67 and a 647 to 703 nm bandpass filter for Alexa647. Images were deconvoluted with Imspector (Max-Planck Innovation, Munich, Germany). Images and the video were generated using the ImageJ 3D Viewer plugin.

Mass spectrometry

EV proteins (8 μg protein per sample) were separated by NuPage Novex 4–12% Bis-Tris gel (Life Technologies), then stained with Coomassie (Bio-Rad, Hercules, CA, USA) for 1 h and destained with water overnight. The 1D SDS-PAGE gel lanes were cut into 2 mm slices with an automatic gel slicer and subjected to in-gel reduction with dithiothreitol, alkylation with iodoacetamide (D4, 98%; Cambridge Isotope Laboratories Inc., Tewksbury, MA, USA), and digestion with trypsin (sequencing grade; Promega, Madison, WI, USA) (27). Nanoflow liquid chromatography coupled to a tandem mass spectrometer (LC-MS/MS) was performed on a Series 1100 capillary LC system (Agilent Technologies, Santa Clara, CA, USA) coupled to an LTQ-Orbitrap XL mass spectrometer (Thermo Scientific, Waltham, MA, USA) operating in positive mode (28). Peptide mixtures were trapped on a ReproSil C18 reverse-phase column (Dr. Maisch GmbH, Ammerbuch-Entringen, Germany; 1.5 cm × 100 μm, packed in house) at a flow rate of 8 μl/min. Peptide separation was performed on ReproSil C18 reversed-phase column (Dr. Maisch GmbH; 15 cm × 50 μm, packed in house) using a linear gradient from 0 to 80% B [A = 0.1% formic acid; B = 80% (v/v) acetonitrile, 0.1% formic acid] in 170 min and at a constant flow rate of 200 nl/min using a splitter. The column eluent was directly sprayed into the electrospray ionization source of the mass spectrometer. Mass spectra were acquired in continuum mode, and fragmentation of the peptides was performed in a data-dependent mode.

Microarray analysis

PC3 cells were incubated with day 12 osteoblast EVs and their controls for 4, 24, and 48 h. Total PC3 cell RNA was isolated using the TRIzol (Life Technologies) extraction method according to the manufacturer's instructions. RNA samples were prepared for microarray analysis using the Illumina TotalPrep RNA Amplification Kit (Ambion; Life Technologies) according to the manufacturer's instructions. Biotinylated cRNA was hybridized to HumanHT-12 v4 Expression BeadChip (Illumina, San Diego, CA, USA) microarray chips according to the manufacturer's protocol. Data acquisition was performed using iScan (Illumina).

Bioinformatic analysis

The raw MS data were analyzed by MaxQuant software (version 1.3.0.5) (29). A false discovery rate of 0.01 for proteins and peptides and a minimum peptide length of 6 amino acids were required. The Andromeda search engine (30) was used to search the MS/MS spectra against the Uniprot database (taxonomy: *Homo sapiens*, release HUMAN_2013_04) concatenated with the reversed versions of all sequences (maximum of 2 missed cleavages; 0.6 Da fragment mass tolerance, enzyme specificity: trypsin). Only proteins identified with at least 2 unique peptides and 2 quantitation events were considered for analysis. The data from the replicates were combined as averages of label-free quantification intensity values for each EV group defined by the mineralization condition and the day of culture. Perseus 1.3.0.4 (Max Planck Institute of Biochemistry, 2012) was used to generate the heat map and scatter plots based on iBAQ values. DAVID Bioinformatics Resources v6.7 was used to categorize the proteins into overrepresented processes using our previously described SV-HFO gene expression data set as a background (31, 32). ExoCarta database (release date: May 29, 2012) was used for comparative EV analysis. Ingenuity (Ingenuity Systems; http://www.ingenuity.com) was used to analyze the interaction between EV proteome and PC3 genes using the path explorer tool in My Pathway analysis.

Statistical analysis

The results were described as mean ± SD based on at least 2 independent experiments. Significance was calculated by a 2-way ANOVA test, and P values of <0.05 were considered significant.

RESULTS

Characterization of human osteoblast EVs during differentiation and under different mineralization conditions

In this study, we used human preosteoblasts (SV-HFOs), which differentiate into mature osteoblasts that produce extracellular matrix and deposit calcium when stimulated with dexamethasone (22). Throughout this study, dexamethasone-treated and non-dexamethasone-treated osteoblasts are referred to as mineralizing (MOB) and nonmineralizing (NMOB) osteoblasts, respectively. To reduce serum-derived EV contamination, we cultured the osteoblasts in medium supplemented with EV-depleted serum followed by serum-free medium for 24 h before EV isolation. Osteoblasts behaved normally under these modified conditions, and they underwent proper differentiation and mineralization, as shown by Alizarin Red S staining of the calcium deposited in the matrix and ALPL activity (**Fig. 1*A*, *B***).

We isolated EVs secreted by both MOBs and NMOBs on days 5, 12, and 19 of culture by a series of ultracentrifugation steps; we refer to these 6 different EV preparations as EV groups. Transmission electron microscopy images showed that osteoblast EVs had irregular and spherical structures in wide ranges of diameters, depending on the stage of differentiation and mineralization (Fig. 1*C*). EVs secreted by NMOBs were more heterogeneous in size (50–1000 nm) than EVs secreted by MOBs (50–250 nm). We further verified the presence of EVs by testing for known EV proteins, such as CD63 and annexin A2 (ANXA2), by Western blot analysis (Fig. 1*D*) (33). We confirmed the presence of matrix vesicles within the EV groups derived

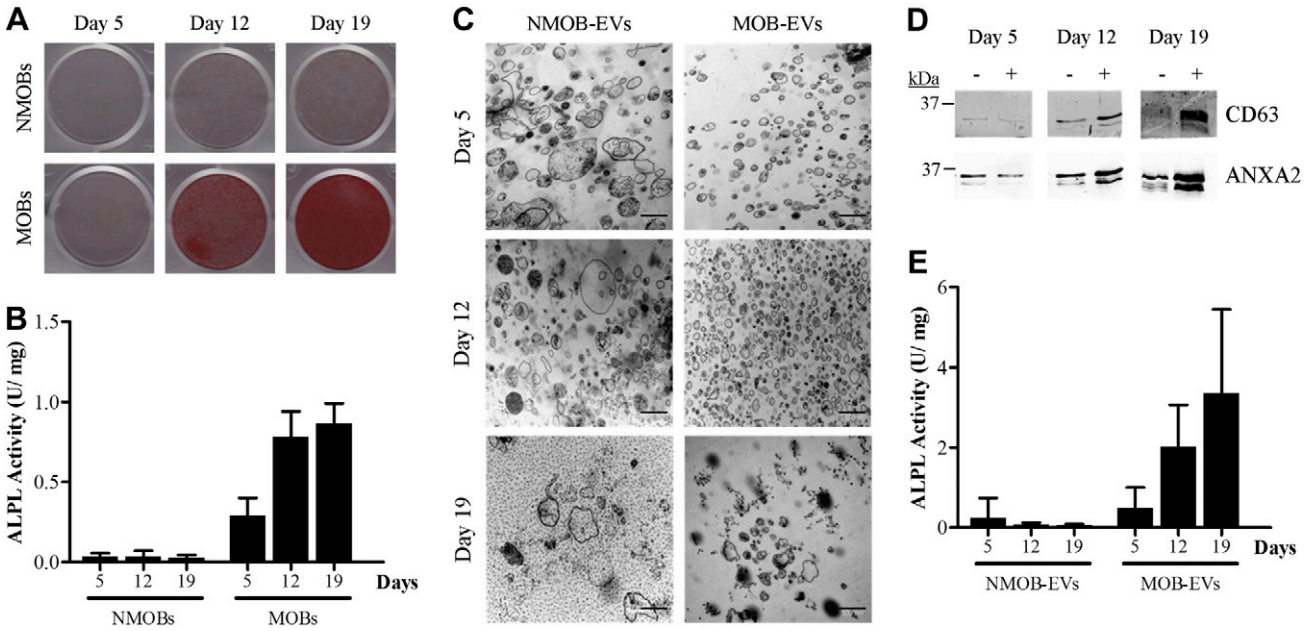

Figure 1. Characterization of EVs secreted by NMOBs and MOBs on days 5, 12, and 19 of culture. *A*) Alizarin Red S staining of the calcium deposited in the bone matrix. *B*) ALPL activity (mean ± SD) of osteoblasts during differentiation. ALPL activity is shown as enzyme unit per milligram (U/mg) of total protein. *C*) Transmission electron microscopy images (original magnification, ×28,000) of each EV group. Scale bar, 500 nm. *D*) Western blot analysis of EV proteins (3 μg/lane) in NMOB-EVs (−) and MOB-EVs (+) using antibodies against CD63 and ANXA2. *E*) ALPL activity (mean ± SD) measured in NMOB-EVs and MOB-EVs (n = 3).

from MOBs by measuring ALPL activity that was absent in EV groups of NMOBs (Fig. 1*E*). These results show that human osteoblasts secrete EVs under both non-mineralizing and mineralizing conditions at different stages of osteoblast differentiation regardless of matrix vesicle activity, suggesting a role not primarily linked to mineralization.

Proteomic profiling of NMOB-EVs and MOB-EVs

EV proteomes of NMOBs and MOBs on days 5, 12, and 19 of culture were analyzed by mass spectrometry, as previously described (28, 34). Briefly, proteins of isolated EVs were separated by SDS-PAGE electrophoresis, in-gel digested, and analyzed by LC-MS/MS. Altogether, we detected 1120 proteins, among which 946 proteins (84%) were detected in every EV group despite the morphologic differences shown in Fig. 1*C*. These proteins consisted of commonly known vesicle proteins and were mainly annotated to a wide array of vesicle-related molecular functions and biologic processes (**Fig. 2*A***). Furthermore, the overlapping proteins included osteoblast-related proteins linked to skeletal development, mesenchymal differentiation, calcium ion binding, and phosphatase activity, which can be attributed to the activity of matrix vesicles (Supplemental Table 1). Figure 2*B* shows a schematic representation of the overrepresented protein families found in all EV groups.

Next, we combined the protein data from all 3 time points for each of the mineralization conditions. The Venn diagram in **Fig. 3*A*** shows that 1090 proteins (97% of the total proteins) were overlapping. Four and 26 proteins were uniquely detected in NMOB-EVs and MOB-EVs, respectively. Comparison with the ExoCarta database (33) showed that the majority of the mineralization condition-specific proteins (3 of 4 NMOB-EV and 22 of 26 MOB-EV proteins) as well as 352 overlapping proteins were uniquely detected in our osteoblast EVs at the time of the analysis (Fig. 3*A*). Gene ontology (GO) annotation analysis indicated that these osteoblast-specific proteins were mostly annotated to ribonucleoprotein complex, RNA binding, ribosome, initiator factor, and nucleotide binding (Fig. 3*B*). **Table 1** lists the osteoblast-specific proteins that were uniquely detected in either NMOB-EVs or MOB-EVs. Together, these findings show that osteoblast EVs are enriched with known vesicular proteins while they also contain unique proteins depending on the mineralization condition.

Label-free quantitative distribution of osteoblast EV proteins

Absolute protein abundances can be estimated by label-free methods based on quantification using the peak intensities of the LC-MS/MS data. We used the iBAQ values from the MaxQuant analysis output to identify the most abundant proteins in each EV group and compared the protein abundances between the different EV groups (35). The most abundant EV proteins were the commonly known vesicular proteins, such as ANXA2, GAPDH, CD9, ENO1, and PDCD61P, for all EV groups (**Fig. 4*A***) (33). Interestingly, all EV groups contained

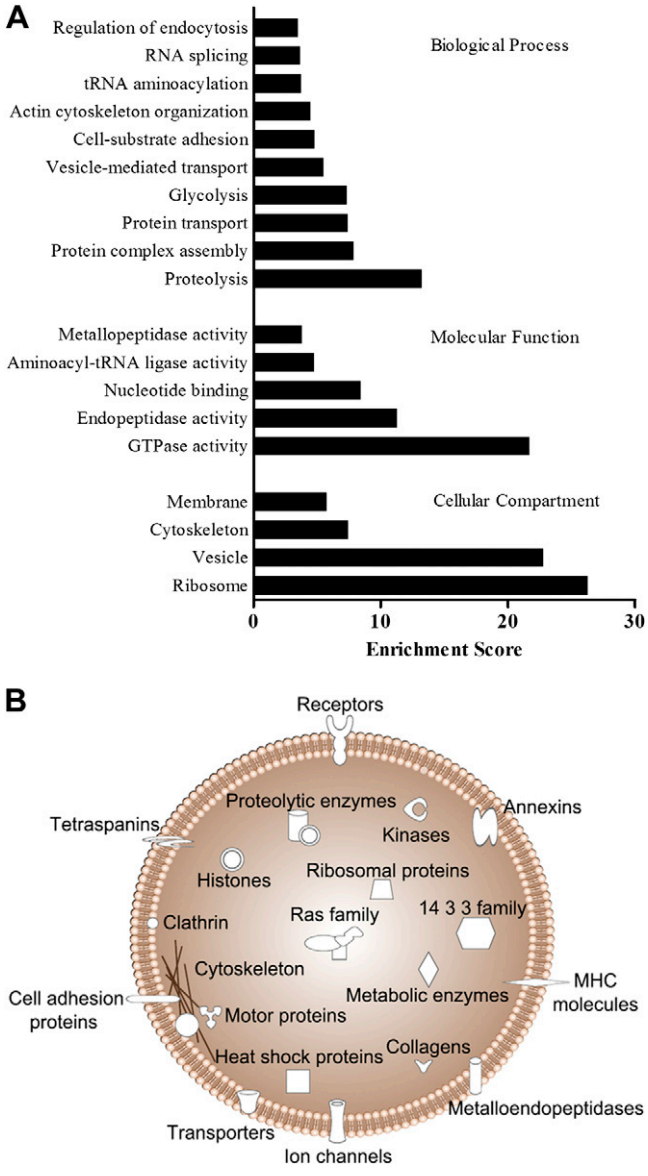

Figure 2. Protein profiling of NMOB-EVs and MOB-EVs on days 5, 12, and 19 of culture. *A*) GO annotations for cellular components, molecular functions, and biologic processes of EV proteins shared across the 6 EV groups ($n = 2$). Only the highest significantly (Benjamini $P < 0.001$) overrepresented terms are shown. *B*) Schematic representation of the protein families detected in all EVs determined on the basis of literature and Ingenuity analyses.

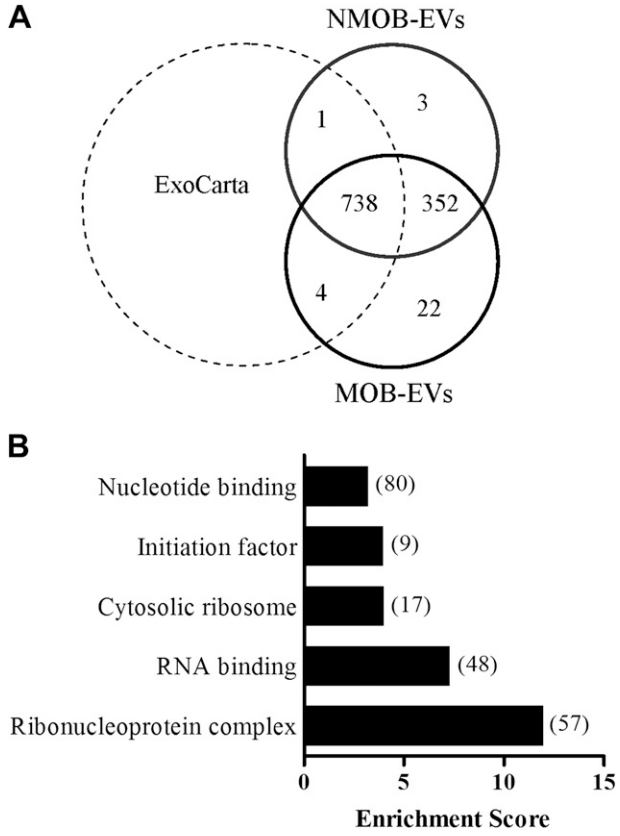

Figure 3. Identification of novel osteoblast-specific EV proteins. *A*) Venn diagram showing numbers of proteins in EVs derived from NMOBs and MOBs and comparison with proteins reported in ExoCarta. *B*) GO annotations of novel osteoblast EV proteins (A) not recorded in ExoCarta. Only the highest significantly (Benjamini $P < 0.001$) overrepresented terms are shown. Brackets indicate number of proteins for each term.

high levels of histones. The multiscatter plots in Fig. 4*B* show a strong correlation between the protein content of the different EV groups. EV proteins isolated at different time points during culture showed a higher correlation when compared within a culture condition (*i.e.,* within NMOBs and MOBs) than between the culture conditions. The differences between EVs derived from NMOBs and MOBs became more apparent as the cells started to mineralize on day 12 (day 5, $r = 0.959$; day 12, $r = 0.912$; day 19, $r = 0.905$).

Next, we compared the average intensities of NMOB-EV and MOB-EV proteins isolated on the same day of culture to identify specifically enriched EV proteins. Proteins with more than 5-fold increase in iBAQ intensities were regarded as more abundant in either one of the EV groups on that specific day of culture (Fig. 4*C–E*). In accordance with the scatter plots, the number of abundant MOB-EV proteins showed a strong increase from 46 to 279 and 321 on day 12 (onset of mineralization) and 19 (full mineralization), respectively (Fig. 4*D, E*). Surprisingly, these proteins were mostly annotated to RNA binding and processing, and not to matrix vesicle–dependent mineralization. NMOB-EVs were mainly enriched with cell adhesion–associated extracellular matrix proteins and chromosomal proteins. **Table 2** provides a representative list of proteins that were detected with more than 5-fold abundance in NMOB-EVs and MOB-EVs. The Venn diagrams in Fig. 4*F* and *G* show the distribution of the proteins (Fig. 4*C–E*) specifically enriched in either NMOB-EVs (Fig. 4*F*) or MOB-EVs (Fig. 4*G*) over the different culture time points. HMGA2, PLAU, TNC, and HIST1H1C were highly abundant at every time point in NMOB-EVs. MOB-EVs were enriched with 22 proteins throughout culture, among which ALPL and CD109 showed the most striking abundance. These results show that despite the similarity in protein content, osteoblast EVs are enriched with distinct proteins depending on the mineralization condition and the stage of differentiation.

TABLE 1. *List of osteoblast-specific proteins uniquely detected in either NMOB-EVs or MOB-EVs*

Osteoblast	UniProt accession	Gene symbol	Description
NMOB-EV	Q9BUB4	*ADAT1*	tRNA-specific adenosine deaminase 1
	P19784	*CSNK2A2*	Casein kinase II subunit alpha
	Q02539	*HIST1H1A*	Histone H1.1
MOB-EV	Q8TDN6	*BRIX1*	Ribosome biogenesis protein BRX1 homolog
	P45973	*CBX5*	Chromobox protein homolog 5
	Q7Z7A1	*CNTRL*	Centriolin
	Q9UBL6	*CPNE7*	Copine-7
	Q9NVP1	*DDX18*	ATP-dependent RNA helicase DDX18
	P23743	*DGKA*	Diacylglycerol kinase alpha
	Q9HCE0	*EPG5*	Ectopic P granules protein 5 homolog
	P46976	*GYG1*	Glycogenin-1
	Q13151	*HNRNPA0*	Heterogeneous nuclear ribonucleoprotein A0
	O00425	*IGF2BP3*	Insulinlike growth factor 2 mRNA-binding protein 3
	O43731	*KDELR3*	ER lumen protein retaining receptor 3
	Q6VAB6	*KSR2*	Kinase suppressor of Ras 2
	O15243	*LEPROT*	Leptin receptor gene-related protein
	Q9H0P0	*NT5C3*	Cytosolic 5-nucleotidase 3
	Q8TAD7	*OCC1*	Overexpressed in colon carcinoma 1 protein
	Q5T091	*RER1*	Protein RER1
	Q9GZN7	*ROGDI*	Protein rogdi homolog
	P67812	*SEC11A*	Signal peptidase complex catalytic subunit SEC11A
	P61011	*SRP54*	Signal recognition particle 54 kDa protein
	Q13242	*SRSF9*	Serine/arginine-rich splicing factor 9
	O14787	*TNPO2*	Transportin-2
	P11172	*UMPS*	Uridine 5-monophosphate synthase

Effect of osteoblast EVs on PC3 cell growth

We next tested the functionality of EVs in intercellular communication. For this, we chose the osteoblast–prostate tumor cell interaction. Proteomics analyses indicated that the EV proteome content of NMOBs and MOBs started to show greater specificity on day 12 of culture. Therefore, we focused on day 12 EVs. We analyzed whether osteoblast EVs regulate PC3 cell growth and survival *in vitro*. First we evaluated the uptake of osteoblast EVs by PC3 cells using fluorescence labeling. High-resolution 4Pi microscopy analysis confirmed that PC3 cells internalized the PKH67-labeled osteoblast EVs within 24 h (**Fig. 5*A, B***, Supplemental Video). Flow cytometry analyses indicated that EV uptake was dose dependent (Fig. 5*C*).

We then performed microarray analysis to investigate the effect of osteoblast EV treatment on the gene expression profile of PC3 cells. We incubated PC3 cells with day 12 NMOB-EVs and MOB-EVs, and collected RNA after 4, 24, and 48 h. Interestingly, treatment with the 2 different EV groups resulted in regulation of different sets of prostate cancer genes (Supplemental Table 2). We identified 98 and 76 genes that were regulated more than 1.5-fold by NMOB-EVs and MOB-EVs, respectively, compared to the control-treated cells (Fig. 5*D*). The 2 overlapping genes were *FTHL8* and *LOC728499*, and they were down- and up-regulated by both EV groups, respectively. The majority of the genes in both treatment groups were down-regulated (74 of 96 genes by NMOB-EVs and 48 of 74 genes by MOB-EVs). Ingenuity analysis indicated that even though the regulated genes were different, they were annotated to similar molecular and cellular functions mainly related to cell growth and survival ($P < 0.05$). We assessed the effect of osteoblast EVs on PC3 cell growth by culturing the tumor cells with different EV concentrations for 5 d. Both NMOB-EVs and MOB-EVs induced 2-fold increase of absolute cell numbers compared to control-treated cells (Fig. 5*E*).

We used bioinformatics to integrate the proteomics and microarray data, and thus correlate the proteome of day 12 osteoblast EVs to the EV-regulated PC3 genes. We used Ingenuity software to build a network showing the direct molecular relationships between the EV proteins and the regulated PC3 genes for each treatment group (**Fig. 6**). Twenty-five of the 98 NMOB-EV-regulated PC3 genes were mapped with 157 of 980 day 12 NMOB-EV proteins (Fig. 6*A*). The majority of the proteins were annotated to vesicle and ribosomal proteins, and mainly interacted with *YWHAG* and *PAK2*. For the MOB-EV

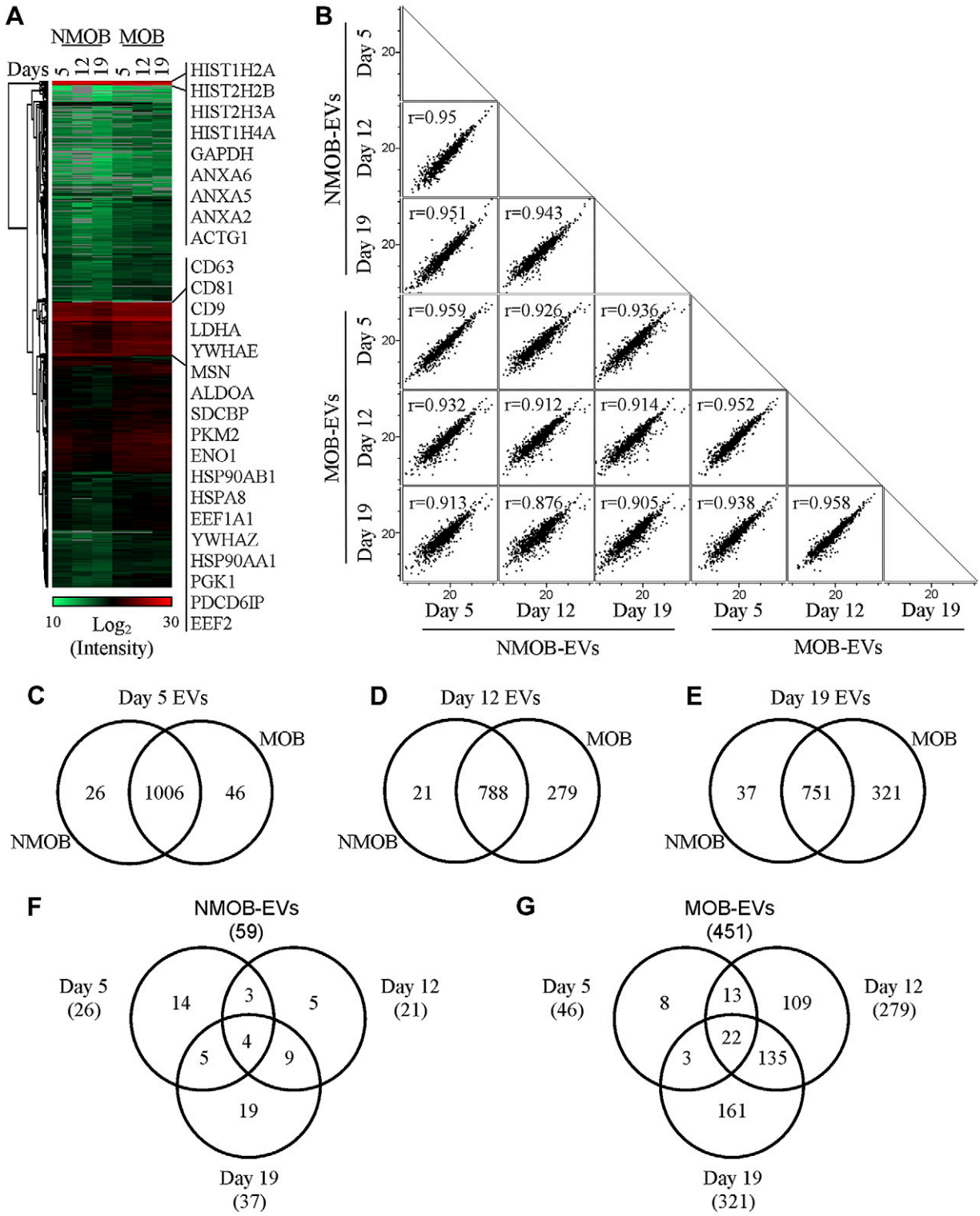

Figure 4. Comparative proteomic analysis of EVs secreted from NMOBs and MOBs during 19 d of culture. *A*) Heat map showing protein abundances (iBAQ values) across the 6 EV groups. The most abundant proteins including the top identified EV markers (ExoCarta) are shown next to the heat map. Red, high abundance; green, low abundance; gray, no signal. *B*) Multiscatter plots show the strong correlation between NMOB-EV and MOB-EV protein abundances. Venn diagrams (*C–G*) show the number of proteins that are at least 5-fold more abundant in either NMOB-EVs or MOB-EVs on (*C*) day 5, (*D*) day 12, and (*E*) day 19, and the distribution of the abundant proteins in (*F*) NMOB-EVs and (*G*) MOB-EVs at different stages of differentiation.

treatment, 38 of 76 genes interacted with 337 proteins of 1079 day 12 MOB-EV proteins (Fig. 6*B*). Most of the mapped proteins were ribosomal proteins and interacted predominantly with *RAD21* and *CDK5*. Together, these results show that NMOB-EVs and MOB-EVs are both internalized by PC3 cells and regulate the expression of different prostate genes, but with both converging to stimulate cell growth.

TABLE 2. *Representative list of proteins significantly enriched (>5-fold) in either NMOB- or MOB-EVs*

Osteoblast	UniProt accession	Gene symbol	Description
NMOB-EV			
Extracellular matrix proteins			
	P08253	*MMP2*	72 kDa type IV collagenase
	P00749	*PLAU*	Urokinase-type plasminogen activator
	Q15582	*TGFBI*	Transforming growth factor β–induced protein ig-h3
	P35442	*THBS2*	Thrombospondin-2
	P24821	*TNC*	Tenascin
	P13611	*VCAN*	Versican core protein
Chromosomal proteins			
	P07305	*H1F0*	Histone H1.0
	P16403	*HIST1H1C*	Histone H1.2
	P62805	*HIST1H4A*	Histone H4
	P17096	*HMGA1*	High mobility group protein HMG-I
	P52926	*HMGA2*	High mobility group protein HMGI-C
MOB-EV			
Ribonucleoprotein complexes			
	Q00839	*HNRNPU*	Heterogeneous nuclear ribonucleoprotein U
	Q12906	*ILF3*	Interleukin enhancer-binding factor 3
	P49207	*RPL34*	60S ribosomal protein L34
	P62847	*RPS24*	40S ribosomal protein S24
	Q92616	*GCN1L1*	Translational activator GCN1
RNA binding proteins			
	Q9NR30	*DDX21*	Nucleolar RNA helicase 2
	Q9Y2L1	*DIS3*	Exosome complex exonuclease RRP44
	P20042	*EIF2S2*	Eukaryotic translation initiation factor 2 subunit 2
	Q01081	*U2AF1*	Splicing factor U2AF 35 kDa subunit
	Q9HAV4	*XPO5*	Exportin-5
Nucleotide binding proteins			
	Q9UN86	*G3BP2*	Ras GTPase-activating protein-binding protein 2
	P54652	*HSPA2*	Heat shock–related 70 kDa protein 2
	O00425	*IGF2BP3*	Insulinlike growth factor 2 mRNA-binding protein 3
	Q14566	*MCM6*	DNA replication licensing factor MCM6
	P22694	*PRKACB*	cAMP-dependent protein kinase catalytic subunit β
GTPase activity			
	P84085	*ARF5*	ADP-ribosylation factor 5
	Q9NZN4	*EHD2*	EH domain–containing protein 2
	P20591	*MX1*	Interferon-induced GTP-binding protein Mx1
	P61020	*RAB5B*	Ras-related protein Rab-5B
	P08134	*RHOC*	Rho-related GTP-binding protein RhoC
Other			
	Q09666	*AHNAK*	Neuroblast differentiation-associated protein AHNAK
	P05186	*ALPL*	Alkaline phosphatase, tissue-nonspecific isozyme
	Q8ND76	*CCNY*	Cyclin-Y; Cyclin-Y-like protein 2
	6YHK3	*CD109*	CD109 antigen
	Q13451	*FKBP5*	Peptidyl-prolyl *cis-trans* isomerase FKBP5

DISCUSSION

The findings described in this study showed that both NMOBs and MOBs secrete EVs selectively packaged with known vesicle proteins as well as an interesting range of proteins unique to the mineralization and differentiation status of the osteoblasts. Osteoblast EVs enter human prostate cancer cells, regulate the expression of cell growth–related prostate cancer genes, and stimulate their growth *in vitro,* demonstrating their active role in intercellular communication.

Osteoblasts actively undergo sequential events of differentiation along the course of their maturation. Previous work by our group showed the importance of studying protein and genetic composition of osteoblasts at different stages of their differentiation (22, 28). Here we used a well-characterized human preosteoblast cell model to isolate EVs at 3 stages of differentiation to gain a comprehensive understanding of the osteoblast EV proteome: premineralization (day 5), onset of mineralization (day 12), and full mineralization (day 19). We also isolated EVs from NMOBs at the same culture time points

as a comparison to elucidate the EV proteins not primarily linked to mineralization and thus understand their role in cell communication. Interestingly, 84% of the total proteins were shared between all the EV groups, and 97% were detected at least in one of the time points in both NMOB-EVs and MOB-EVs. This was surprising because the transmission electron microscopy images showed clear morphologic differences between the EVs secreted by osteoblasts under different mineralization conditions. A large number of the overlapping proteins were novel proteins, primarily associated with ribonucleoproteins, which were not recorded in the EV database ExoCarta at the time of the analysis. Even though we cannot exclude the notion that part of these proteins may be arising from nonspecific background, recent studies reporting the presence of vesicle-associated RNA binding proteins suggest that our osteoblast EVs contain novel proteins linked to known vesicle-related processes (36, 37).

We hypothesized that despite the similarities in cargo, the different EV groups are specifically enriched with distinct proteins, thus providing clues to their biologic function. Label-free quantification is a useful proteomics tool to compare the relative abundances of proteins across different samples, which leads to a selection of proteins that can be analyzed for molecular function. All of the EV groups described in this study contained abundant levels of the classic vesicle proteins, such as annexins (ANXA2, ANXA6), tetraspanins (CD9, CD81), and metabolic proteins (GAPDH, LDHA), thus verifying the robustness of these proteins as vesicle markers. It is interesting to note that histones were also among the highly enriched proteins detected in all EV groups. In fact, we previously showed that histone proteins were among the most abundant proteins in human bone, suggesting the likelihood of possessing extranuclear roles (38). There have been an increasing number of studies reporting the functionality of circulating nuclear proteins as well as their presence in apoptotic bodies, exosomes, and microvesicles (7, 39–41). Although the abundances of the predominant proteins were similar across all EV groups, we detected unique group of proteins that were at least 5-fold more abundant in EVs secreted by either NMOBs or MOBs at a given culture time point. Among the bone-related proteins, ALPL was significantly enriched in MOB-EVs with an increasing abundance in time, which paralleled the vesicular and cellular ALPL activity. Mineralization is indeed one of the most important processes of bone formation, with a major role for matrix vesicles. Thus, it is not surprising to observe the high level of vesicular ALPL activity in MOB-EVs compared to the donor cells. However, the GO analyses showing overrepresentation of vesicle-related processes over bone-related processes suggested a role for EVs not primarily linked to mineralization. The most striking differences

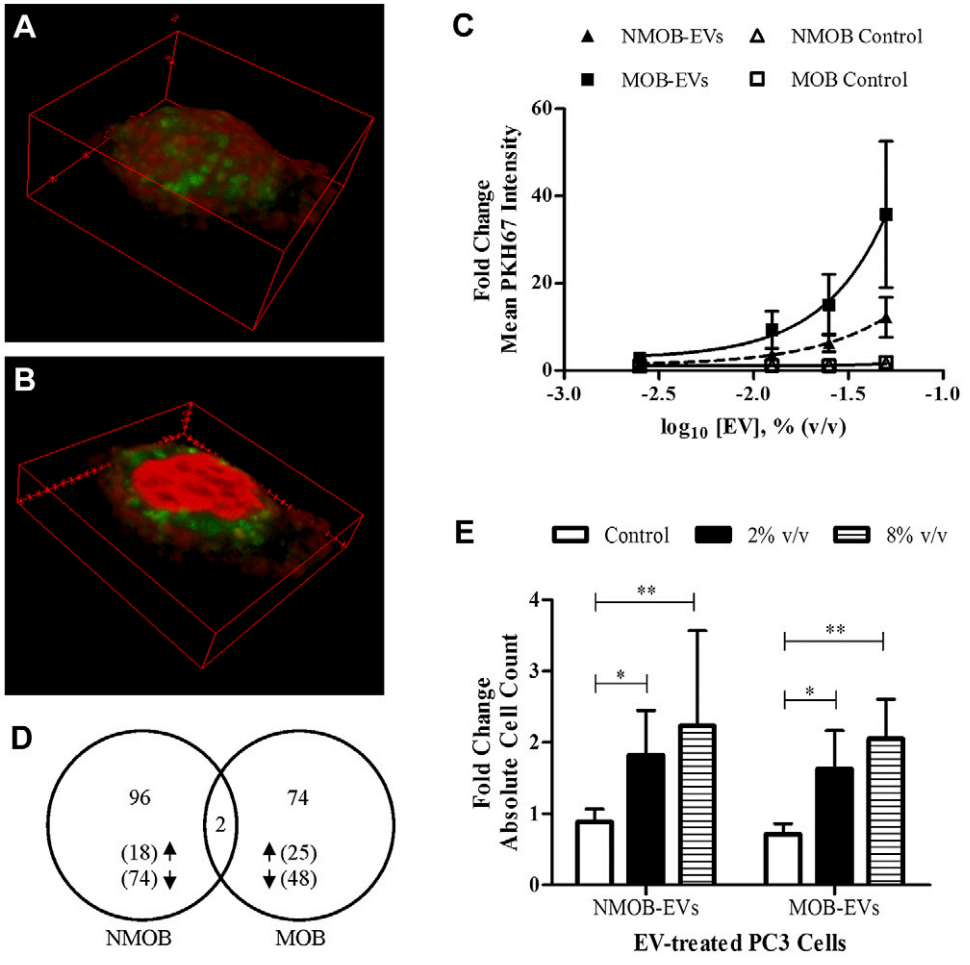

Figure 5. Internalization of day 12 osteoblast EVs and their functional effect on PC3 cells. *A* and *B*) 4Pi images showing the uptake of PKH67-labeled NMOB-EVs by PC3 cells. *A*) A 3-D reconstruction of all confocal stacks. *B*) Half plane showing the EVs inside the cells. Images are representative for MOB-EVs uptake. Red, cell membrane and nucleus; green, PKH67-labeled EVs (Supplemental Movie). *C*) Flow cytometry analysis shows dose-dependent uptake (mean ± SD) of PKH67-labeled EVs by PC3 cells ($n = 2$). Fold change is determined relative to untreated cells. *D*) Venn diagram showing PC3 genes regulated in response to day 12 osteoblast EVs (2.86% v/v) by at least 1.5-fold. Numbers in brackets denote the genes that were up- and down-regulated by the respective EV group. *E*) Fold change of PC3 cell count (mean ± SD) after 5 d of incubation with different EV doses ($n = 3$). $^*P < 0.05$, $^{**}P < 0.01$. Control, cell-free culture medium processed the same way as conditioned medium.

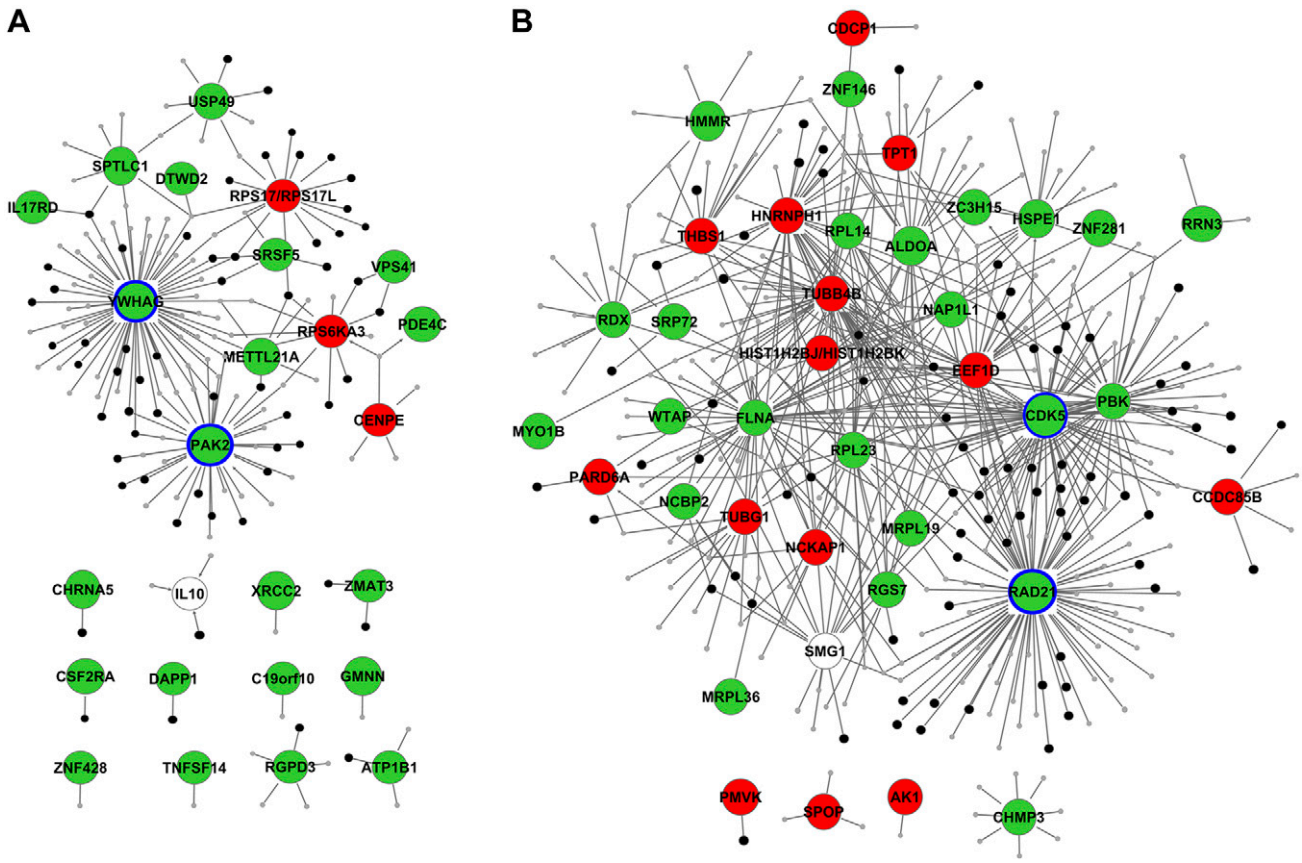

Figure 6. Ingenuity network analysis showing the direct relationship maps between the EV-regulated PC3 genes and day 12 EV proteins for (*A*) NMOB-EV and (*B*) MOB-EV treatments. Green, down-regulated PC3 genes; red, up-regulated PC3 genes; gray, EV proteins; black, EV proteins annotated to vesicles and ribosomes. The most predominantly mapped PC3 genes are highlighted (blue line).

between the EV groups were the enrichment of adhesion proteins and RNA binding proteins in NMOB-EVs and MOB-EVs, respectively.

To investigate the role of EVs in intercellular communication, we tested EV uptake by prostate cancer cells and their effect on prostate cancer cell growth. Prostate cancer, which is one of the most frequently diagnosed cancers among men, is primarily associated with bone metastasis (42). Osteoblast microenvironment consisting of a network of receptors and secreted factors acts as an attractive force and regulator of tumor cell growth (43). We showed that PC3 prostate cancer cells dose-dependently internalized PKH67-labeled EVs derived from both NMOBs and MOBs. The fluorescence intensity of PC3 cells treated with MOB-EVs was higher than those treated with NMOB-EVs at any given EV dose. Because of the challenges of absolute quantification of EVs, it is difficult to make an accurate quantitative comparison between the EV groups (44). Moreover, the mode of internalization may contribute to the difference in fluorescence signal. EVs that are internalized *via* endocytosis are more likely to retain a stronger PKH67 signal compared to the EVs that transfer their cargo *via* fusion in a host cell's plasma membrane. Here, we observed that osteoblast EVs retained their fluorescence upon overnight culture. Therefore it seems that endocytosis is involved in their uptake; however, we cannot rule out the involvement of other uptake modes.

Studying the molecular mechanism of cancer survival and growth is an important area of investigation. In particular, bone metastasis, which is considered an incurable stage of the disease, is of great interest with clinical significance. Our EV treatment studies demonstrated that both NMOB-EVs and MOB-EVs stimulated the growth of PC3 cells *in vitro*. This shows that osteoblast EVs are not only internalized by the prostate cancer cells but also that they are functional and can stimulate prostate cancer cell growth. This was further supported by PC3 cell gene expression analysis, which revealed the EV-regulated prostate cancer genes were mainly involved in cell survival and growth. It is important to note that the 2 EV groups affected the regulation of different sets of prostate cancer genes, which were annotated to similar molecular functions. This was most likely due to the differences in their bioactive cargo, which may act *via* different pathways but lead to the same biologic outcome.

Proteomic analyses showed that there are differences in protein abundances between day 12 NMOB-EVs and MOB-EVs. When we mapped the EV proteins with the regulated prostate genes in an interaction network, we found that the MOB-EV-regulated genes were mostly mapped with ribosomal and RNA binding proteins. Previous studies showed the role of ribosomal proteins in physiologic events, such as proliferation and cell growth, besides the well-known role in protein

biosynthesis (45). Lai and Xu (46) showed that ribosomal proteins are also involved in cancer progression and metastasis. In particular, ribosomal proteins have been shown to have elevated expression levels in prostate tumors and hence play an important role in prostate cancer development (47, 48). NMOB-EV-regulated genes were mostly mapped with known vesicle proteins, mainly consisting of signaling proteins and chaperones, as well as ribosomal proteins that may act *via* different pathways than the MOB-EV proteins. The 14-3-3 family proteins are involved in various signaling cascades and have been shown to be regulators of prostate cancer tumor formation with the exception of 14-3-3σ protein, a tumor suppressor, which is, most interestingly, not present in osteoblast EVs (49, 50). Chaperones such as heat shock proteins have been shown to be negative regulators of apoptosis during prostate tumorigenesis, suggesting an antiapoptotic role for our chaperone-containing osteoblast EVs (51). With the growing interest in the field, more comprehensive information on EV composition and knowledge of their molecular function in diverse biologic and pathologic processes is becoming of utmost importance. Alternatively, increasing reports on EV biogenesis, content, and targeting may provide the basis for their exploitation as carriers of therapeutic cargo for targeted cancer therapy, cell therapy, and tissue engineering (52–54). In this study, we demonstrated that osteoblast EVs play a role in the cross-talk between osteoblasts and prostate cancer cells, highlighting the importance of EV cargo in cancer regulation. We anticipate that deeper investigation of EV function in the bone microenvironment will help us develop preventive or curative therapies for a broad range of pathologic conditions.

In conclusion, our data provide insights into the morphology and proteomic composition of osteoblast EVs at different stages of differentiation under mineralizing and nonmineralizing conditions. The proteomic analyses presented here suggest a role for osteoblast EVs in intercellular communication besides a well-characterized role in mineralization. We further demonstrate the existence of an EV-driven interaction between osteoblasts and prostate cancer cells, stressing the clinical/pathophysiological significance of our data. Challenges still remain, however, because we need optimized tools to quantify and separate different subpopulations of EVs and to interpret the roles of individual proteins in the context of communication. The present study unequivocally demonstrates that osteoblasts produce EVs that can enter other cells and stimulate their proliferation. This provides an additional way by which osteoblasts may regulate their microenvironment—not only in metastatic prostate cancer cells but also in the surrounding bone marrow cells, such as hematopoietic stem cells and osteoclasts. FJ

This work was supported by a grant from the Dutch government to the Netherlands Institute for Regenerative Medicine (NIRM, Grant FES0908), Erasmus MC Stem Cell and Regenerative Medicine Institute, and Erasmus Medical Center. The authors thank M.C.G. Bourgondien for assisting with electron microscopy, and K. Bezstarosti and D. Dekkers for mass spectrometry analysis.

REFERENCES

1. Marks, S. C., Jr., and Popoff, S. N. (1988) Bone cell biology: the regulation of development, structure, and function in the skeleton. *Am. J. Anat.* **183**, 1–44
2. Chamberlain, G., Fox, J., Ashton, B., and Middleton, J. (2007) Concise review: mesenchymal stem cells: their phenotype, differentiation capacity, immunological features, and potential for homing. *Stem Cells* **25**, 2739–2749
3. Proff, P., and Römer, P. (2009) The molecular mechanism behind bone remodelling: a review. *Clin. Oral Investig.* **13**, 355–362
4. Taichman, R. S. (2005) Blood and bone: two tissues whose fates are intertwined to create the hematopoietic stem-cell niche. *Blood* **105**, 2631–2639
5. Coleman, R. E. (2006) Clinical features of metastatic bone disease and risk of skeletal morbidity. *Clin. Cancer Res.* **12**, 6243s–6249s
6. Shiozawa, Y., Pedersen, E. A., Havens, A. M., Jung, Y., Mishra, A., Joseph, J., Kim, J. K., Patel, L. R., Ying, C., Ziegler, A. M., Pienta, M. J., Song, J., Wang, J., Loberg, R. D., Krebsbach, P. H., Pienta, K. J., and Taichman, R. S. (2011) Human prostate cancer metastases target the hematopoietic stem cell niche to establish footholds in mouse bone marrow. *J. Clin. Invest.* **121**, 1298–1312
7. Théry, C., Ostrowski, M., and Segura, E. (2009) Membrane vesicles as conveyors of immune responses. *Nat. Rev. Immunol.* **9**, 581–593
8. Morhayim, J., Baroncelli, M., and van Leeuwen, J. P. (2014) Extracellular vesicles: specialized bone messengers. [E-pub ahead of print] *Arch. Biochem. Biophys.* 10.1016/j.abb.2014.05.011
9. Raposo, G., and Stoorvogel, W. (2013) Extracellular vesicles: exosomes, microvesicles, and friends. *J. Cell Biol.* **200**, 373–383
10. Shifrin, D. A., Jr., Demory Beckler, M., Coffey, R. J., and Tyska, M. J. (2013) Extracellular vesicles: communication, coercion, and conditioning. *Mol. Biol. Cell* **24**, 1253–1259
11. Ratajczak, M. Z., Kucia, M., Jadczyk, T., Greco, N. J., Wojakowski, W., Tendera, M., and Ratajczak, J. (2012) Pivotal role of paracrine effects in stem cell therapies in regenerative medicine: can we translate stem cell–secreted paracrine factors and microvesicles into better therapeutic strategies? *Leukemia* **26**, 1166–1173
12. Katsuda, T., Kosaka, N., Takeshita, F., and Ochiya, T. (2013) The therapeutic potential of mesenchymal stem cell–derived extracellular vesicles. *Proteomics* **13**, 1637–1653
13. Tetta, C., Bruno, S., Fonsato, V., Deregibus, M. C., and Camussi, G. (2011) The role of microvesicles in tissue repair. *Organogenesis* **7**, 105–115
14. Ostrowski, M., Carmo, N. B., Krumeich, S., Fanget, I., Raposo, G., Savina, A., Moita, C. F., Schauer, K., Hume, A. N., Freitas, R. P., Goud, B., Benaroch, P., Hacohen, N., Fukuda, M., Desnos, C., Seabra, M. C., Darchen, F., Amigorena, S., Moita, L. F., Thery, C. (2010) Rab27a and Rab27b control different steps of the exosome secretion pathway. *Nat. Cell Biol.* **12**, 19–30
15. Al-Nedawi, K., Meehan, B., and Rak, J. (2009) Microvesicles: messengers and mediators of tumor progression. *Cell Cycle* **8**, 2014–2018
16. Hristov, M., Erl, W., Linder, S., and Weber, P. C. (2004) Apoptotic bodies from endothelial cells enhance the number and initiate the differentiation of human endothelial progenitor cells in vitro. *Blood* **104**, 2761–2766
17. Anderson, H. C., Garimella, R., and Tague, S. E. (2005) The role of matrix vesicles in growth plate development and biomineralization. *Front. Biosci.* **10**, 822–837
18. Xiao, Z., Camalier, C. E., Nagashima, K., Chan, K. C., Lucas, D. A., de la Cruz, M. J., Gignac, M., Lockett, S., Issaq, H. J., Veenstra, T. D., Conrads, T. P., and Beck, G. R., Jr. (2007) Analysis of the extracellular matrix vesicle proteome in mineralizing osteoblasts. *J. Cell. Physiol.* **210**, 325–335
19. Balcerzak, M., Malinowska, A., Thouverey, C., Sekrecka, A., Dadlez, M., Buchet, R., and Pikula, S. (2008) Proteome analysis of matrix vesicles isolated from femurs of chicken embryo. *Proteomics* **8**, 192–205
20. Thouverey, C., Malinowska, A., Balcerzak, M., Strzelecka-Kiliszek, A., Buchet, R., Dadlez, M., and Pikula, S. (2011) Proteomic

characterization of biogenesis and functions of matrix vesicles released from mineralizing human osteoblast-like cells. *J. Proteomics* **74**, 1123–1134
21. Nahar, N. N., Missana, L. R., Garimella, R., Tague, S. E., and Anderson, H. C. (2008) Matrix vesicles are carriers of bone morphogenetic proteins (BMPs), vascular endothelial growth factor (VEGF), and noncollagenous matrix proteins. *J. Bone Miner. Metab.* **26**, 514–519
22. Eijken, M., Koedam, M., van Driel, M., Buurman, C. J., Pols, H. A., and van Leeuwen, J. P. (2006) The essential role of glucocorticoids for proper human osteoblast differentiation and matrix mineralization. *Mol. Cell. Endocrinol.* **248**, 87–93
23. Bruedigam, C., Driel, M., Koedam, M., Peppel, J., van der Eerden, B. C., Eijken, M., and van Leeuwen, J. P. (2011) Basic techniques in human mesenchymal stem cell cultures: differentiation into osteogenic and adipogenic lineages, genetic perturbations, and phenotypic analyses. *Curr. Protoc. Stem Cell Biol.* Chapter 1, Unit1H 3 doi:10.1002/9780470151808.sc01h03s17
24. Glaschick, S., Röcker, C., Deuschle, K., Wiedenmann, J., Oswald, F., Mailänder, V., and Nienhaus, G. U. (2007) Axial resolution enhancement by 4Pi confocal fluorescence microscopy with two-photon excitation. *J. Biol. Phys.* **33**, 433–443
25. van Cappellen, A. W., Nigg, A., and Houtsmuller, A. B. (2012) *Enhancement of Optical Rsolution by 4Pi Single and Multiphoton Confocal Fluorescence Microscopy,* Academic Press, Oxford
26. Hell, S., and Stelzer, E. H. K. (1992) Fundamental improvement of resolution with a 4Pi-confocal fluorescence microscope using 2-photon excitation. *Opt. Commun.* **93**, 277–282
27. Wilm, M., Shevchenko, A., Houthaeve, T., Breit, S., Schweigerer, L., Fotsis, T., and Mann, M. (1996) Femtomole sequencing of proteins from polyacrylamide gels by nano-electrospray mass spectrometry. *Nature* **379**, 466–469
28. Alves, R. D., Eijken, M., Swagemakers, S., Chiba, H., Titulaer, M. K., Burgers, P. C., Luider, T. M., and van Leeuwen, J. P. (2010) Proteomic analysis of human osteoblastic cells: relevant proteins and functional categories for differentiation. *J. Proteome Res.* **9**, 4688–4700
29. Cox, J., Matic, I., Hilger, M., Nagaraj, N., Selbach, M., Olsen, J. V., and Mann, M. (2009) A practical guide to the MaxQuant computational platform for SILAC-based quantitative proteomics. *Nat. Protoc.* **4**, 698–705
30. Cox, J., Neuhauser, N., Michalski, A., Scheltema, R. A., Olsen, J. V., and Mann, M. (2011) Andromeda: a peptide search engine integrated into the MaxQuant environment. *J. Proteome Res.* **10**, 1794–1805
31. Huang da, W., Sherman, B. T., and Lempicki, R. A. (2009) Systematic and integrative analysis of large gene lists using DAVID bioinformatics resources. *Nat. Protoc.* **4**, 44–57
32. Eijken, M., Swagemakers, S., Koedam, M., Steenbergen, C., Derkx, P., Uitterlinden, A. G., van der Spek, P. J., Visser, J. A., de Jong, F. H., Pols, H. A., and van Leeuwen, J. P. (2007) The activin A–follistatin system: potent regulator of human extracellular matrix mineralization. *FASEB J.* **21**, 2949–2960
33. Mathivanan, S., Fahner, C. J., Reid, G. E., and Simpson, R. J. (2012) ExoCarta 2012: database of exosomal proteins, RNA and lipids. *Nucleic Acids Res.* **40**, D1241–D1244
34. Stoop, M. P., Lamers, R. J., Burgers, P. C., Sillevis Smitt, P. A., Hintzen, R. Q., and Luider, T. M. (2008) The rate of false positive sequence matches of peptides profiled by MALDI MS and identified by MS/MS. *J. Proteome Res.* **7**, 4841–4847
35. Schwanhäusser, B., Busse, D., Li, N., Dittmar, G., Schuchhardt, J., Wolf, J., Chen, W., and Selbach, M. (2011) Global quantification of mammalian gene expression control. *Nature* **473**, 337–342
36. Collino, F., Deregibus, M. C., Bruno, S., Sterpone, L., Aghemo, G., Viltono, L., Tetta, C., and Camussi, G. (2010) Microvesicles derived from adult human bone marrow and tissue specific mesenchymal stem cells shuttle selected pattern of miRNAs. *PLoS ONE* **5**, e11803
37. Meckes, D. G., Jr., Gunawardena, H. P., Dekroon, R. M., Heaton, P. R., Edwards, R. H., Ozgur, S., Griffith, J. D., Damania, B., and Raab-Traub, N. (2013) Modulation of B-cell exosome proteins by gamma herpesvirus infection. *Proc. Natl. Acad. Sci. USA* **110**, E2925–E2933
38. Alves, R. D., Demmers, J. A., Bezstarosti, K., van der Eerden, B. C., Verhaar, J. A., Eijken, M., and van Leeuwen, J. P. (2011) Unraveling the human bone microenvironment beyond the classical extracellular matrix proteins: a human bone protein library. *J. Proteome Res.* **10**, 4725–4733
39. Hosseini-Beheshti, E., Pham, S., Adomat, H., Li, N., and Tomlinson Guns, E. S. (2012) Exosomes as biomarker enriched microvesicles: characterization of exosomal proteins derived from a panel of prostate cell lines with distinct AR phenotypes. *Mol. Cell. Proteomics* **11**, 863–885
40. Sun, N. K., and Chao, C. C. (2005) The cytokine activity of HMGB1—extracellular escape of the nuclear protein. *Chang Gung Med. J.* **28**, 673–682
41. Bab, I., Gazit, D., Chorev, M., Muhlrad, A., Shteyer, A., Greenberg, Z., Namdar, M., and Kahn, A. (1992) Histone H4–related osteogenic growth peptide (OGP): a novel circulating stimulator of osteoblastic activity. *EMBO J.* **11**, 1867–1873
42. Roodman, G. D. (2004) Mechanisms of bone metastasis. *N. Engl. J. Med.* **350**, 1655–1664
43. Joyce, J. A., and Pollard, J. W. (2009) Microenvironmental regulation of metastasis. *Nat. Rev. Cancer* **9**, 239–252
44. Varga, Z., Yuana, Y., Grootemaat, A. E., van der Pol, E., Gollwitzer, C., Krumrey, M., and Nieuwland, R. (2014) Towards traceable size determination of extracellular vesicles. *J Extracell Vesicles* Feb 4;3 doi:10.3402/jev.v3.23298
45. Wool, I. G. (1996) Extraribosomal functions of ribosomal proteins. *Trends Biochem. Sci.* **21**, 164–165
46. Lai, M. D., and Xu, J. (2007) Ribosomal proteins and colorectal cancer. *Curr. Genomics* **8**, 43–49
47. Wang, M., Hu, Y., and Stearns, M. E. (2009) RPS2: a novel therapeutic target in prostate cancer. *J. Exp. Clin. Cancer Res.* **28**, 6
48. Vaarala, M. H., Porvari, K. S., Kyllönen, A. P., Mustonen, M. V. J., Lukkarinen, O., and Vihko, P. T. (1998) Several genes encoding ribosomal proteins are over-expressed in prostate-cancer cell lines: confirmation of L7a and L37 over-expression in prostate-cancer tissue samples. *Int. J. Cancer* **78**, 27–32
49. Oh, S., Shin, S., Lightfoot, S. A., and Janknecht, R. (2013) 14-3-3 proteins modulate the ETS transcription factor ETV1 in prostate cancer. *Cancer Res.* **73**, 5110–5119
50. Urano, T., Takahashi, S., Suzuki, T., Fujimura, T., Fujita, M., Kumagai, J., Horie-Inoue, K., Sasano, H., Kitamura, T., Ouchi, Y., and Inoue, S. (2004) 14-3-3sigma is down-regulated in human prostate cancer. *Biochem. Biophys. Res. Commun.* **319**, 795–800
51. Ciocca, D. R., Fanelli, M. A., Cuello-Carrion, F. D., and Castro, G. N. (2010) Heat shock proteins in prostate cancer: from tumorigenesis to the clinic. *Int. J. Hyperthermia* **26**, 737–747
52. Ohno, S., Takanashi, M., Sudo, K., Ueda, S., Ishikawa, A., Matsuyama, N., Fujita, K., Mizutani, T., Ohgi, T., Ochiya, T., Gotoh, N., and Kuroda, M. (2013) Systemically injected exosomes targeted to EGFR deliver antitumor microRNA to breast cancer cells. *Mol. Ther.* **21**, 185–191
53. Zhang, Y., Li, L., Yu, J., Zhu, D., Zhang, Y., Li, X., Gu, H., Zhang, C. Y., and Zen, K. (2014) Microvesicle-mediated delivery of transforming growth factor β1 siRNA for the suppression of tumor growth in mice. *Biomaterials* **35**, 4390–4400
54. van Dommelen, S. M., Vader, P., Lakhal, S., Kooijmans, S. A., van Solinge, W. W., Wood, M. J., and Schiffelers, R. M. (2012) Microvesicles and exosomes: opportunities for cell-derived membrane vesicles in drug delivery. *J. Control. Release* **161**, 635–644

Received for publication August 5, 2014.
Accepted for publication September 15, 2014.